ELSEVIER

Journal of Alloys and Compounds 224 (1995) 70–75

Journal of ALLOYS AND COMPOUNDS

The site occupancies for the excess manganese atoms and the third element niobium in the intermetallic compound $ZrMn_2$

T. Kodama, H. Anada, H. Kaminaka

Sumitomo Metal Industries Ltd., 1-8 Fusocho, Amagasaki, Hyogo, 660 Japan

Received 5 October 1993; in final form 17 October 1994

Abstract

The site occupancies for the stoichiometric excess of Mn atoms and the third element Nb in the hexagonal C14-Laves type $ZrMn_2$ were studied by investigating systematic changes of the lattice parameters and the broadenings of diffracted X-ray profiles with the chemical compositions for $ZrMn_x$ ($x=0.98$–2.89) and $Zr(Mn_{1-y}Nb_y)_x$ ($x=0.97$–2.91, $y=0.036$–0.212) alloys. The excess Mn atoms in $ZrMn_x$ alloys (hypo-Zr) occupy the A sites in the hexagonal C14-Laves type AB_2 crystal. Nb atoms in $Zr(Mn_{1-y}Nb_y)_x$ alloys (hyper-Zr) occupy the B sites. Nb atoms in $Zr(Mn_{1-y}Nb_y)_x$ alloys (hypo-Zr) are substituted for Mn atoms in the A sites until Mn atoms in the A sites are exhausted. They turn to occupy the B sites after Mn atoms in the A sites are exhausted.

Keywords: Site occupancies; Manganese atoms; Third element niobium; Intermetallic compounds

1. Introduction

The intermetallic compound $ZrMn_2$ is one of the hydrogen-absorbing materials that is characterized by easy activation and rapid reaction with hydrogen at relatively high temperatures. The authors have shown that additions of the third element Nb into the Zr–Mn alloy systems lower the hydrogen equilibrium pressures and expand the lattice parameters for the $ZrMn_2$ crystal [1], and that they change the hydrogen capacities of the Zr–Mn alloys [2]. It is necessary to clarify the site occupancies for the alloying atoms in order to explain their influence on the hydriding properties of the alloys. About this subject in Zr–Mn alloy systems, Sinha *et al.* [3] and Pourarian *et al.* [4–6] measured the densities and the lattice parameters for the non-stoichiometric $ZrMn_2T_x$ (T=Mn, Fe, Co, Ni, Cu) and $ZrMn_{2.8}T_x$ (T=Fe, Ni) alloys, concluding that no vacancy existed at the Zr sites and that the stoichiometric excess of Mn atoms or the third element occupied the Zr sites instead of the interstitial sites. By neutron diffraction experiments, Pontonnier et al. [7] established that the stoichiometric excess of Mn atoms occupied the Zr sites and Triantafillidis et al. [8] established that Fe atoms in $Zr(Mn_{1-y}Fe_y)_x$(hypo Zr) occupied the Mn sites.

The site occupancy for Nb atoms in the $ZrMn_2$ compound is unknown. It is expected that the site occupancy for Nb atoms can be analyzed by the Rietveld method [7–9]. But in this work the site occupancy has been estimated by a simple method, in which it has been supposed that the lattice parameters and the diffracted X-ray profiles for the $ZrMn_2$ crystal in $ZrMn_x$ and $Zr(Mn_{1-y}Nb_y)_x$ alloys will show systematic changes depending on the chemical compositions, because it has been estimated that the site occupancy will change with the chemical composition and that the lattice parameters and the lattice strains are related to the site occupancies for the constituent atoms.

2. Experimental methods

Small ingots of about 0.15 kg were melted by arc melting under an argon atmosphere. The ingots were remelted upside down after the first melting for homogenization. The raw materials for melting were reactor-grade zirconium sponge, electrolytic manganese and electrolytic niobium.

The constituent elements in the ingots were analysed by inductively coupled plasma mass spectrometry. The chemcial composition was reduced to the formula $ZrMn_x$ or $Zr(Mn_{1-y}Nb_y)_x$, even if the alloy had two phases, $ZrMn_2$ and α-Zr.

The chemical compositions of the alloys were as follows:

SSDI 0925-8388(94)01473-6

(1) $ZrMn_x$

11 charges; $x = 0.98$–2.89.

(2) $Zr(Mn_{1-y}Nb_y)_x$

22 charges; $x = 0.97$–2.91, $y = 0.036$–0.212.

8 alloy series including $ZrMn_x$:

$Zr(Mn_{1-y}Nb_y)_{1.0}$, $Zr(Mn_{1-y}Nb_y)_{1.2}$,

$Zr(Mn_{1-y}Nb_y)_{1.7}$, $Zr(Mn_{1-y}Nb_y)_{1.9}$,

$Zr(Mn_{1-y}Nb_y)_{2.2}$, $Zr(Mn_{1-y}Nb_y)_{2.4}$,

$Zr(Mn_{1-y}Nb_y)_{2.6}$, $Zr(Mn_{1-y}Nb_y)_{2.9}$.

The combinations of x and y are plotted on the xy plane in Fig. 1.

The ingot was divided into several blocks. The blocks were heat-treated before grinding for the X-ray diffraction test. Heat-treatment conditions were several, in order to study their effects on the lattice parameters and the half widths. Heat-treatment conditions were as follows:

(1) As-cast condition

(2) Annealed condition

1073 K×5 h in vacuum

1273 K×5 h in vacuum

1323 K×72 h in vacuum

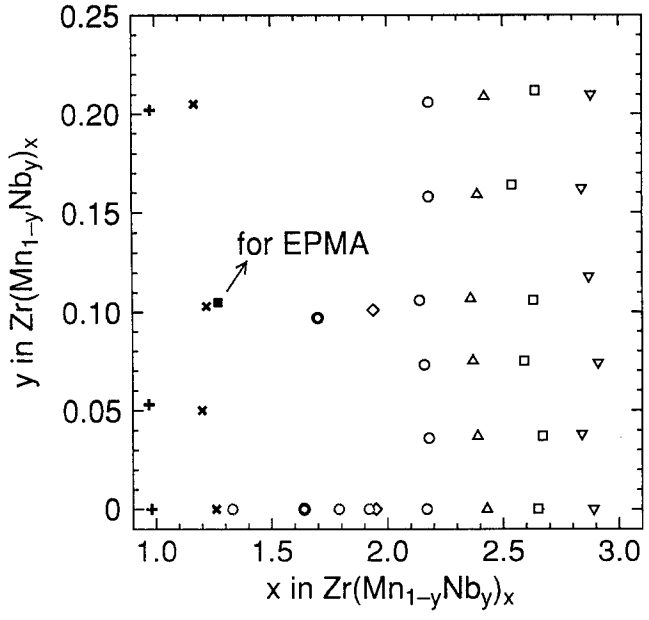

Fig. 1. The measured chemical compositions x and y for $ZrMn_x$ and $Zr(Mn_{1-y}Nb_y)_x$ alloys: +, $Zr(Mn_{1-y}Nb_y)_{1.0}$; ×, $Zr(Mn_{1-y}Nb_y)_{1.2}$; ●, $Zr(Mn_{1-y}Nb_y)_{1.7}$; ◇, $Zr(Mn_{1-y}Nb_y)_{1.9}$; ○, $Zr(Mn_{1-y}Nb_y)_{2.2}$; △, $Zr(Mn_{1-y}Nb_y)_{2.4}$; □, $Zr(Mn_{1-y}Nb_y)_{2.6}$; ▽ $Zr(Mn_{1-y}Nb_y)_{2.9}$; ■, for EPMA only.

(3) Oil-quenched condition ($ZrMn_{0.98}$ and $ZrMn_{1.33}$)

1273 K×5 h → OQ in vacuum

All specimens except the oil-quenched specimens were furnace-cooled to room temperature in vacuum after annealing at high temperatures. This took about 4 h.

The blocks were powdered by grinding in the argon atmosphere. The size of the powder was about 10 μm. Powdered specimens were tested by X-ray diffraction using mono-chromated Co Kα radiation in order to identify the crystals in the alloys and to obtain the lattice parameters and the broadening of the diffracted X-ray profiles from the crystals.

The lattice parameters were measured by the method of least squares. The diffraction angle was calibrated by Si powder. The peak position of a profile was determined by second derivative for the profile. Radius r_S, derived from volume per atom, known as the Seitz radius and expressing the atomic sizes of the elements [10,11], was used as a comparative measure of the lattice parameters. The Seitz radius was obtained from the lattice parameters as follows:

$$\frac{4}{3}\pi r_S^3 = \frac{\text{volume of the unit cell}}{\text{number of atoms in the cell}}$$

The broadening of the diffracted X-ray profiles from the $ZrMn_2$ compound was measured as the half-widths [$\Delta(2\theta)$ at half maximum] for the diffraction profiles from (110), (103), (112) and (201) planes, which showed comparatively stronger intensity. The half widths were determined on the chart after profile refinement. The four values were arithmetically averaged.

The preliminary examinations of the effects of annealing after pulverization on the half widths for the representative specimens were carried out. The annealing condition was 1073 K×5 h in vacuum. The results were as shown in Table 1. Differences between "as-pulverized" and "annealed after pulverization" were hardly recognized. The X-ray diffraction tests have been carried out, therefore, on the as-pulverized powders.

The $Zr(Mn_{0.895}Nb_{0.105})_{1.27}$ alloy was analysed in the as-cast and annealed (1273 K×5 h) conditions by electron probe microanalysis (EPMA) for the element distributions. The preparations of the specimens for EPMA were as follows:

(1) A small piece was buried in the synthetic resin.

Table 1

Specimen [a]	As-pulverized	Annealed
$ZrMn_{2.65}$	0.39°	0.39°
$Zr(Mn_{0.79}Nb_{0.21})_{2.17}$	0.94°	0.90°

[a] Annealed (1273 K×5 h in vacuum) before pulverization.

(2) The buried sample was polished on wet abrasive papers, and then on a cotton cloth containing the hydrogen peroxide.
(3) The polished sample was etched with the fluoronitric acid solution.

3. Results

3.1. $ZrMn_x$ alloys

Parts of the X-ray patterns for the as-cast $ZrMn_x$ alloys ($x=2.17$–2.89) and the annealed are shown in Fig. 2. There were no differences between the as-cast and annealed specimens. Both the $ZrMn_2$ phase (hexagonal C14-Laves type [12]) and the α-Zr phase were present in the alloys with $x<2$. The intensities of the X-ray reflections from the α-Zr phase decreased with increasing x. Only the $ZrMn_2$ phase was observed in the alloys with $x=2.17$–2.89. No α-Mn phase was observed in the alloys investigated.

The Seitz radii and the half-widths for $ZrMn_x$ alloys are shown in Fig. 3. The Seitz radii decreased gradually and monotonically in the range $x \geqslant 1.64$ with increasing x. The half widths seem to have a minimum value near $x=2$ (stoichiometric composition) and have an increasing tendency in the range of $x>2$. The heat treatments showed no effects on both the Seitz radii and the half widths.

Oxygen contents in the as-cast $ZrMn_{1.64}$ and $ZrMn_{1.79}$ alloys were 0.08–0.09% in weight. Those in the same alloys annealed for 72 h at 1323 K were 0.09%. The above Seitz radii and the half widths for the heat-treated alloys have been free from oxidation, because no or negligible oxidation has occurred during annealing.

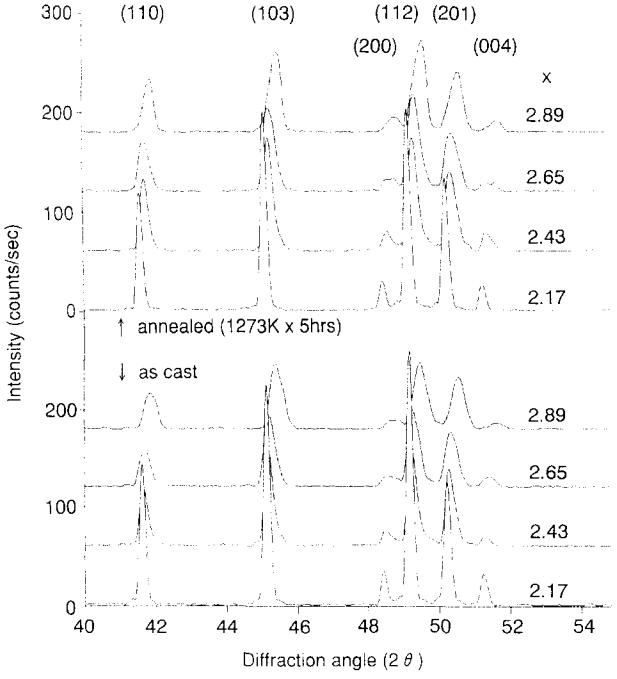

Fig. 2. Parts of the X-ray patterns for the as-cast and annealed $ZrMn_x$ alloys for four values of x.

3.2. $Zr(Mn_{1-y}Nb_y)_x$ alloys

The phases identified in these alloys by X-ray diffraction were the same as those in $ZrMn_x$ alloys. Neither α-Mn nor α-Nb was observed in the range from $x=0.97$ to $x=2.91$.

The element distributions in the annealed $Zr(Mn_{0.895}Nb_{0.105})_{1.27}$ alloy are shown in Fig. 4. Nb atoms seem to be distributed mainly in the Zr–Mn phase. The element distributions in the as-cast specimens were the same as in Fig. 4. The structures in both specimens were quantitatively analyzed by energy-dispersive X-ray analysis. The results, which have been continued for both specimens, are as follows:

Zr-Mn phase:

$$Zr(Mn_{0.905\pm0.007}Nb_{0.095\pm0.007})_{1.95\pm0.05}$$

α-Zr phase in the eutectoid structure:

$$Zr_{0.836\pm0.029}Mn_{0.081\pm0.024}Nb_{0.083\pm0.024}$$

It is thus deduced that most of the third element Nb is distributed in the $ZrMn_2$ phase.

Parts of the X-ray patterns for the as-cast $Zr(Mn_{1-y}Nb_y)_{2.9}$ alloy series are shown in Fig. 4. The Seitz radii and the half widths for the alloy series with $x<2$ are shown in Fig. 3(b) and those for the alloy series with $x>2$ are shown in Fig. 3(c). There are no differences between the as-cast and annealed conditions. As described in Section 3.1, no differences have been observed between as-cast and various heat-treatment conditions in $ZrMn_x$ alloys. It is, therefore, derived that both the as-cast specimens and the heat-treated specimens are in thermodynamical equilibrium.

The effects of the Nb content on the Seitz radii and the half widths induced different behaviours in the lower-x ($x<2$) and higher-x ($x>2$) alloy series. The Seitz radii and the half widths for the alloy series with $x<2$ increase monotonically with increasing Nb content. The half widths for the $Zr(Mn_{1-y}Nb_y)_{1.9}$ alloy series are affected most strongly. Those for the alloy series with $x>2$ indicate two-stage change. In the lower y the Seitz radii show slow increases and the half widths show decreasing tendencies. In the higher y, on the other hand, the Seitz radii show steep increases as the alloy series with $x<2$, and the half widths show rapid increases as the alloy series with $x=1.9$.

4. Discussion

4.1. $ZrMn_x$ alloys

The Seitz radii for Zr and Mn atoms by King [12] are 0.1771 and 0.1428 nm respectively, and atomic radii

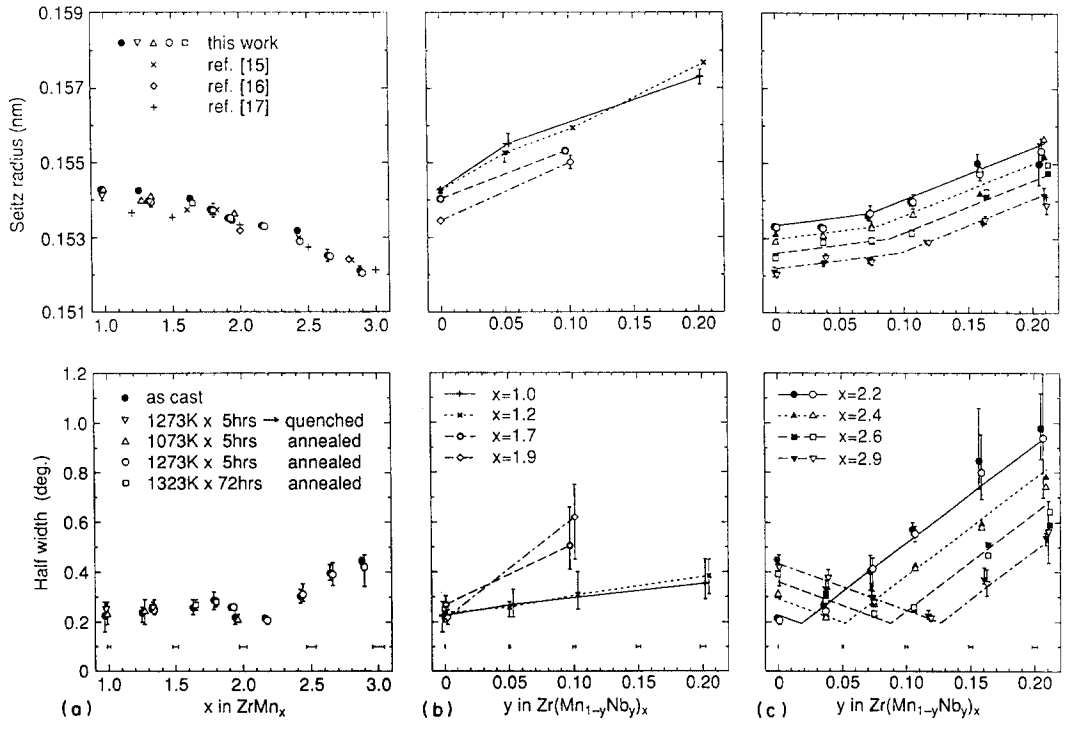

Fig. 3. (a) The Seitz radii and the half widths for the $ZrMn_x$ alloys. x for the as-cast specimen is displaced through -0.01, and that for the annealed $+0.01$. The vertical bars on the graph of the Seitz radius represent one standard deviation. Almost all of them are within the symbols. The standard deviation in (c) was about twice as large as that in (a). The vertical bars on the graph of the half width are for the maximum and minimum. The horizontal bars on that graph represent two standard deviations in chemical analysis. (b) The Seitz radii and the half widths for the as-cast lower-x $Zr(Mn_{1-y}Nb_y)_x$ alloy series. The vertical and horizontal bars are the same as those in (a). (c) The Seitz radii and the half widths and regression lines for the higher-x $Zr(Mn_{1-y}Nb_y)_x$ alloy series. Nb atoms replace Mn atoms in the A sites in the lower-y sides of the intersecting points, while they occupy the B sites in the higher-y sides. Filled symbols are for the as-cast specimens and open ones for the annealed (1273 K×5 h). y for the as-cast $Zr(Mn_{1-y}Nb_y)_{2.2}$ and $Zr(Mn_{1-y}Nb_y)_{2.9}$ are displaced through -0.001 and those for the annealed $+0.001$. The vertical and horizontal bars are the same as those in (a). The error bars for the alloy series $Zr(Mn_{1-y}Nb_y)_{2.4}$ and $Zr(Mn_{1-y}Nb_y)_{2.6}$ are abbreviated for unity.

for them with coordination number of 12 by Pauling [18] are 0.1597 and 0.1268 nm respectively. It is, therefore, expected that the Seitz radii will decrease and the lattice strains increase if Mn atoms occupy the site for Zr atoms. It is derived that the excess Mn atoms occupy the A sites (the site occupancy for Zr atoms in the stoichiometric $ZrMn_2$), because only the $ZrMn_2$ phase exists in these alloys, and because the Seitz radii decrease and the half widths increase with increasing x ($x>2$). This result is the same as that for the site occupancy for the excess Mn atoms by Sinha *et al.* [3] and Pontonnier et al. [7]. The partition of the composing elements in $ZrMn_x$ (hypo-Zr) alloy into the occupancy sites is, therefore, shown by the following expression:

$$ZrMn_x (x>2) \longrightarrow (Zr_{1-a}Mn_a)Mn_2$$

$$a = \frac{x-2}{x+1} \qquad (1)$$

4.2. $Zr(Mn_{1-y}Nb_y)_x$ alloys

4.2.1. Site occupancy for Nb atoms in hyper-Zr alloys and stoichiometric alloys

It is estimated by the results of the X-ray diffractions and EPMA on the $Zr(Mn_{0.895}Nb_{0.105})_{1.27}$ alloy that most of the third element Nb is distributed in the $ZrMn_2$ phase. Both the Seitz radii and the half widths increased rapidly with increasing Nb content. It is derived, therefore, that Nb atoms are substituted for the smaller atoms than Nb atoms (the Seitz radius for the Nb atom is 0.1625 nm [12] and the atomic radius with a coordination number of 12 is 0.1456 nm [18]). It is, consequently, deduced that Nb atoms occupy the B sites (the site occupancy for Mn atoms in the stoichiometric $ZrMn_2$).

The increase of the half widths with y is smaller in the lower-x alloy series ($x=1.0$ and 1.2 in Fig. 3(b)). When the larger Nb atoms are substituted for the smaller Mn atoms, it is expected that the strain caused by the substitution is smaller if the Seitz radius for the original crystal is larger. The Seitz radius for the lower-x alloy is larger than that for the higher-x alloy, as shown in Fig. 3(a), so that the above consideration seems to be valid.

4.2.2. Site occupancy for Nb atoms in hypo-Zr alloys

The Seitz radii increase slowly and the half widths decrease at the first stage (i.e. at the lower Nb content).

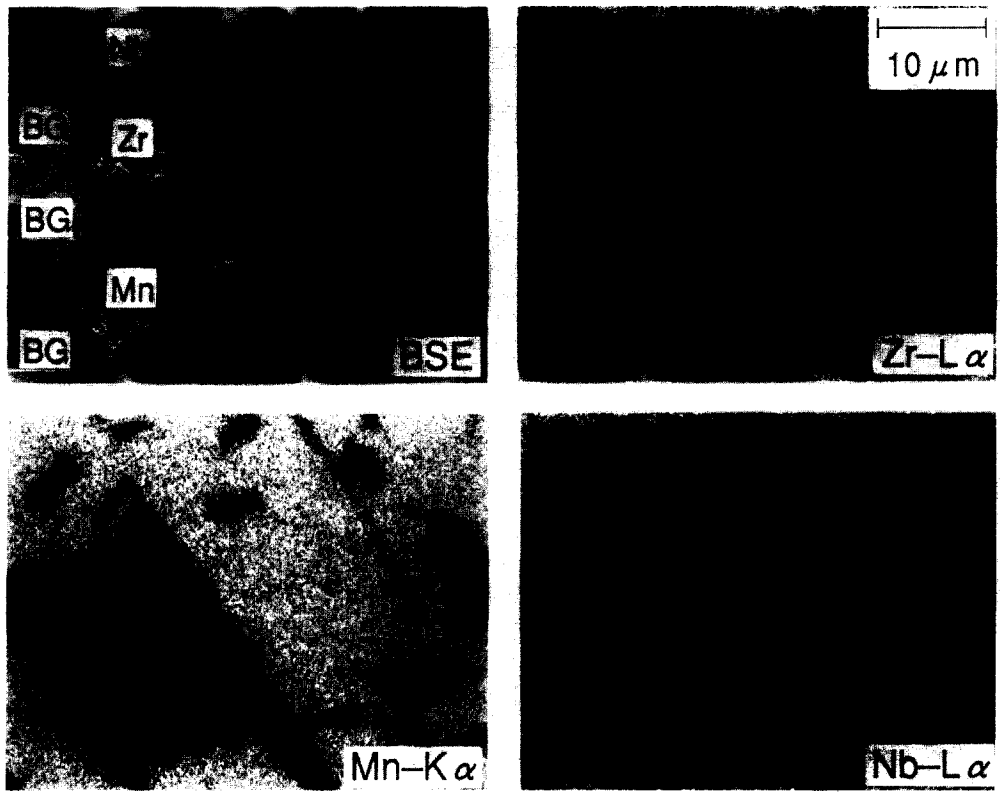

Fig. 4. The element distributions by EPMA in $Zr(Mn_{0.895}Nb_{0.105})_{1.27}$ alloy annealed for 5 h at 1273 K. The lines on the BSE (backscattered electron) image show distributions for Mn, Zr and Nb along the horizontal straight line in the middle. The short lines under the distribution lines show the backgrounds (BG) for each element.

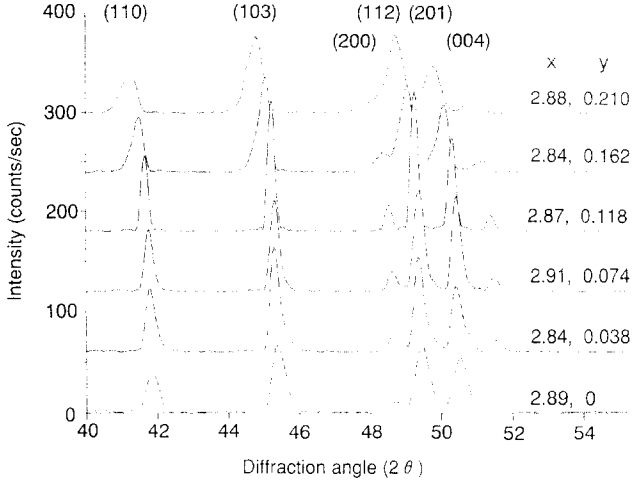

Fig. 5. Parts of the X-ray patterns for the as-cast $Zr(Mn_{1-y}Nb_y)_{2.9}$ alloy series.

It is, consequently, estimated that the first stage is the process in which Nb atoms are substituted for smaller atoms which have produced the lattice strain, and the larger Nb atoms relax the strain. So it is derived that Nb atoms are substituted for Mn atoms that have occupied the A sites.

In the second stage the Seitz radii and the half widths start to increase rapidly. The slopes are almost the same as those of the $Zr(Mn_{1-y}Nb_y)_{1.9}$ alloy series shown in Fig. 3(b). It is, therefore, estimated that Nb atoms are in this stage substituted for Mn atoms that have occupied the B sites.

If no other phase exists except AB_2 in $Zr(Mn_{1-y}Nb_y)_x$ alloy ($x>2$), then $Zr(Mn_{1-y}Nb_y)_x$ can be expressed as follows:

$$Zr(Mn_{1-y}Nb_y)_x\ (x>2) \longrightarrow (Zr_{1-a-b}Mn_aNb_b)(Mn_{1-c}Nb_c)_2$$

$$a+b=\frac{x-2}{x+1}$$

$$b+2c=\frac{3xy}{x+1} \qquad (2)$$

These equations can be solved for a, b and c on the condition that Nb atoms are preferentially substituted for Mn atoms in the A sites, and that they turn to occupy the B sites after Mn atoms in the A sites have been exhausted.

The regression lines about four alloy series with $x=2.2$, 2.4, 2.6 and 2.9 have been calculated on the basis of the above discussions and the assumption that each line for the lower y (higher y) has a common gradient. The alloys have been divided into the lower-y and higher-y groups according to the theoretical relation for the boundary y', which is the Nb content

at which Mn atoms in the A sites are just exhausted. The boundary y' is calculated by the next relation and shown in Fig. 6.

$$Zr(Mn_{1-y'}Nb_{y'})_x\ (x>2) \longrightarrow (Zr_{1-b'}Nb_{b'})Mn_2$$

$$y' = \frac{x-2}{3x} \qquad b' = \frac{x-2}{x+1} \tag{3}$$

The regression expressions and the intersection lines have been obtained as follows (r is the correlation coefficient):

The Seitz radius r_S (nm)	r
r_S (lower y) $= -0.00164x + 0.00441y + 0.15691$	0.95
r_S (higher y) $= -0.00196x + 0.01386y + 0.15690$	0.96
Intersection line $y = 0.03384x + 0.00021$	
The half width HW (deg.)	r
HW (lower y) $= 0.294x - 1.861y - 0.410$	0.97
HW (higher y) $= -0.604x + 3.921y + 1.435$	0.98
Intersection line $y = 0.155x - 0.319$	

The regression lines are shown in Fig. 3(c) and the intersection lines are shown in Fig. 6. The intersection line for "the Seitz radii" is somewhat deviated from the theoretical curve near $x=2.2$. This deviation is probably caused by the fact that a slight error makes a large displacement of the intersection line, because y in the regression expressions has the same sign for both lower y and higher y. The intersection line for "the half widths" agrees well with the theoretical curve.

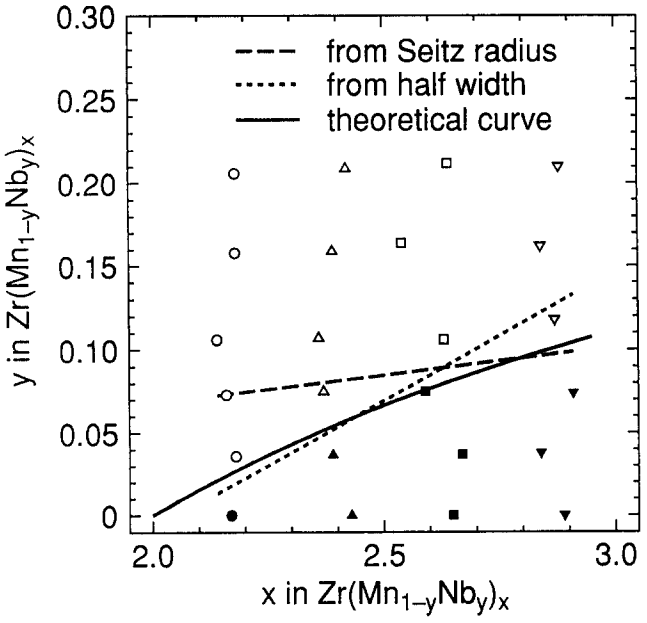

Fig. 6. The intersection line of the regression lines for the lower-y and higher-y groups. Filled symbols are for the lower-y alloys used for the lower-y regression expression and open ones are for the higher-y alloys.

5. Conclusions

(1) The site occupancies for the stoichiometric excess of Mn atoms and the third element Nb atoms in the hexagonal C14-Laves type $ZrMn_2$ crystal lattice were derived from the systematic changes of the lattice parameters and the lattice strains for the $ZrMn_2$ crystal in $ZrMn_x$ and $Zr(Mn_{1-y}Nb_y)_x$ alloys, of which chemical compositions were systematically prepared.

(2) Excess Mn atoms in $ZrMn_x$ alloys (hypo-Zr) occupy the A sites in the hexagonal C14-Laves type AB_2 crystal.

(3) Nb atoms in $Zr(Mn_{1-y}Nb_y)_x$ alloys (hyper-Zr) occupy the B sites.

(4) Nb-atoms in $Zr(Mn_{1-y}Nb_y)_x$ alloys (hypo-Zr) are substituted for Mn atoms in the A sites until Mn atoms in the A sites are exhausted, while they turn to occupy the B sites after Mn atoms in the A sites are exhausted.

References

[1] T. Kodama, H. Anada and H. Yoshinaga, in *MRS International Meeting on Advanced Materials*, 1989, Vol. 2, pp. 57–62.
[2] T. Kodama and H. Kaminaka, to be published.
[3] V.K. Sinha, F. Pourarian and W.E. Wallance, *J. Phys. Chem.*, *86* (1982) 4952–4956.
[4] F. Pourarian, V.K. Sinha and W.E. Wallance, *J. Phys. Chem.*, *86* (1982) 4956–4958.
[5] F. Pourarian and W.E. Wallace, *Solid State Commun.*, *45* (1983) 223–225.
[6] F. Pourarian, V.K. Sinha and W.E. Wallace, *J. Less-Common Met.*, *96* (1984) 237–248.
[7] L. Pontonnier, S. Miraglia, D. Fruchart, J.L. Soubeyroux, A. Baudry and P. Boyer, *J. Alloys Comp.*, *186* (1992) 241–248.
[8] G. Triantafillidis, L. Pontonnier, D. Fruchart, P. Wolfers and J.L. Soubeyroux, *J. Less-Common Met.*, *172–174* (1991) 183–190.
[9] H.M. Rietveld, *Acta Crystallogr.*, *22* (1967) 151–152.
[10] H.M. Rietveld, *J. Appl. Crystallogr.*, *2* (1969) 65–71.
[11] D.B. Willes and R.A. Young, *J. Appl. Cyrstallogr.*, *14* (1981) 149–151.
[12] H.W. King, *J. Mater. Sci.*, *1* (1966) 79–90.
[13] C.S. Barrett and T.B. Massalski, *Structure of Metals*, McGraw-Hill Inc., 3rd edn., 1966.
[14] H.J. Wallbaum, *Z. Kristallogr.*, *103* (1941) 391–402.
[15] R.M. van Essen and K.H.J. Buschow, *Mater. Res. Bull.*, *15* (1980) 1149–1155.
[16] F. Pourarian, H. Fujii, W.E. Wallace, V.K. Sinha and H. Kevin Smith, *J. Phys. Chem.*, *85* (1981) 3105–3111.
[17] W. Luo, J.D. Clewley and T.B. Flanagan, *J. Alloys Comp.*, *185* (1992) 321–338.
[18] L. Pauling, *The Nature of the Chemical Bond*, Cornell University Press, 1960.